

Effects of surface oxidation on the exchange-bias properties of the single-crystal antiferromagnetic/ferromagnetic junction Mn/Co/Cu(001)

M. Caminale,^{1,*} R. Moroni,^{2,†} P. Torelli,³ G. Panaccione,³ W. C. Lin,⁴ M. Canepa,¹ L. Mattera,¹ and F. Bisio²

¹*Dipartimento di Fisica, Università di Genova and CNISM, Sede Consorzziata di Genova, Via Dodecaneso 33, I-16146 Genova, Italy*

²*CNR-SPIN, Corso Perrone 24, I-16152 Genova, Italy*

³*Laboratorio TASC, IOM-CNR, Strada Statale 14 km 163.5, Basovizza, I-34149 Trieste, Italy*

⁴*Department of Physics, National Taiwan Normal University, 116 Taipei, Taiwan*

(Received 9 December 2014; published 31 March 2015)

The effects of a chemical alteration of the antiferromagnet surface in the exchange-biased ultrathin epitaxial antiferromagnetic/ferromagnetic bilayer Mn/Co/Cu(001) have been investigated. The formation of a nanometer-thick paramagnetic oxide at the surface of the Mn layer was induced through the controlled exposure to oxygen. Although the buried Mn/Co interface was not affected by the oxidation, strong changes of the exchange-bias properties of the system, which cannot be accounted for by the mere reduction of the antiferromagnetic Mn thickness, were observed. We propose that the produced surface modification affects the magnetic configuration of the near-surface region and the domain structure in the whole antiferromagnet layer which, in turn, influences the pinned uncompensated spin density responsible for the exchange bias.

DOI: [10.1103/PhysRevB.91.094435](https://doi.org/10.1103/PhysRevB.91.094435)

PACS number(s): 75.70.Ak, 75.30.Et, 75.50.Ee

The exchange-bias (EB) effect manifests as a shift along the magnetic-field axis of the hysteresis loop of antiferromagnetic/ferromagnetic (AF/FM) exchange-coupled systems following field-cooling (FC) procedures [1–5]. The discovery of EB has unleashed a flurry of experimental and theoretical research, motivated by its tremendous technological impact and by the ongoing search for its basic mechanisms [3–5]. The occurrence of EB is nowadays connected with the exchange interactions at the AF/FM interface and the existence of pinned uncompensated (PU) magnetic moments within the AF material. The magnitude of the EB is related to the density of PU magnetic moments, i.e., the magnitude of the uncompensated magnetization of the AF material which, being insensitive to external magnetic fields, represents the symmetry breaking element at the origin of the effect [6].

For a long time, the general consensus was that PU spins were located at the AF/FM interface. Recent works have challenged this intuitive picture, suggesting that PU spins may instead be arranged all over the AF layer, even far from the interface [7–10]. Thus, recent EB studies have begun scrutinizing in ever more depth the spin structure of the AF layer as a whole, thus highlighting the relation between the spin structure and the arrangement of uncompensated spins in the AF [11,12]. In this respect, in ultrathin AF layers, both AF interfaces may contribute to determine the overall AF magnetic structure and therefore the PU-spin density, thus entitling the AF surface layers to play an active role in EB. However, no experimental confirmation of this possibility has been so far reported.

Here, we address the effect of a controlled oxidation of the AF surface layers on the EB properties of the epitaxial AF/FM junction Mn/Co/Cu(001). Mn/Co/Cu(001) is a prototypical system for EB studies thanks to the high-quality layer-by-layer epitaxial growth of both the Co and Mn layers, which

allows the fabrication of structurally and morphologically almost ideal AF/FM junctions [13–17]. In Mn/Co/Cu(001), a sizable EB is observed for Mn thickness (t_{Mn}) above 7–8 monolayers (ML), which increases with increasing t_{Mn} up to about 20 ML and saturates at higher thickness [13]. The oxidation of the metallic Mn layer leads to the formation of a paramagnetic layer at the film surface which shifted upwards the critical Mn thickness for the onset of EB by an amount roughly equal to the thickness of metallic Mn which underwent the oxidation. Interestingly, however, although the surface and buried interface are well separated, a reduction of the high-thickness saturation value of the exchange-bias field was observed, suggesting that modifying the outermost Mn interface, from metal/vacuum to metal/oxide, affected the magnetic structure of the whole AF layer, resulting in a net decrease of the PU-spin density.

The experiments were performed in two surface-science apparatuses, equipped with standard ultrathin-film fabrication and characterization techniques. The former features *in situ* magneto-optical Kerr effect (MOKE) [18], while the latter is the high-energy end station of the Advanced Photoemission Experiment (APE) at the Elettra synchrotron radiation source, equipped with x-ray absorption spectroscopy (XAS), x-ray magnetic circular dichroism (XMCD), and x-ray photoelectron spectroscopy (XPS) instrumentation [19].

A clean and ordered Cu(001) substrate was prepared by cycles of 1-keV Ar⁺ sputtering and annealing at 800 K. Co films of 8-ML thickness were evaporated on Cu(001) at room temperature (RT) by molecular-beam epitaxy (MBE). Mn films were grown by MBE at 250 K on the Co/Cu(001) film in the form of wedges, with Mn thickness between 0 and 25 monolayers [see scheme in Fig. 1(a)]. The pressure in both chambers was systematically below 5×10^{-10} mbar even during evaporation or annealing.

We initially address the chemical properties of the pristine and oxidized samples. In Fig. 1(a), we report the XAS spectrum at the Mn $L_{2,3}$ edges of the as-deposited Mn/Cu/Cu(001) for $t_{\text{Mn}} \approx 18$ ML. The XAS measurements were performed in total electron yield mode, with the sample illuminated by the

*Present address: Max-Planck Institut für Mikrostrukturphysik, Weinberg 2, D-06120 Halle (Saale), Germany.

†Corresponding author: riccardo.moroni@spin.cnr.it

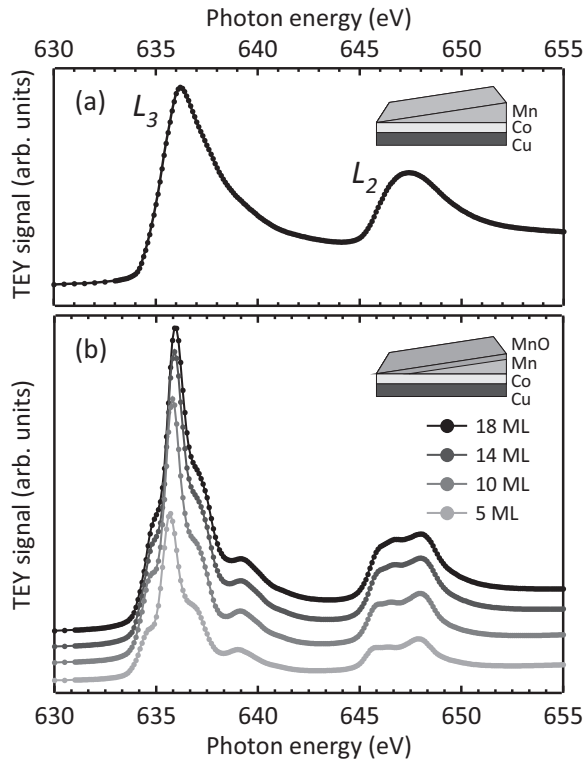


FIG. 1. Top panel: XAS spectrum at the Mn- $L_{2,3}$ edges of as-deposited Mn/Co/Cu(001), collected for $t_{\text{Mn}} \approx 18$ ML. Inset: scheme of the sample geometry. Bottom panel: Mn-thickness dependent XAS spectra at the Mn- $L_{2,3}$ edges of Mn/Co/Cu(001) after exposure to 20 L of O_2 . Spectra corresponding to 5, 10, 14, and 18 ML are shown. The spectra are displaced along the vertical axis for clarity. Inset: sample geometry following the oxidation (see text for details).

incident circularly polarized x-ray beam at 60° from the sample normal. The XAS spectrum exhibits smooth and rounded peaks in correspondence of both Mn L_3 and L_2 edges, as expected for metallic Mn. The cleanness of the sample was further proven by wide-range and high-resolution XPS measurements, reported in the Appendix.

Under these conditions, the sample could therefore be represented as a *purely metallic* Mn wedge grown onto 8-ML Co/Cu(001). Indeed, no Mn-thickness dependence of the XAS-spectrum shape could be observed for the as-deposited Mn/Co/Cu(001) in the investigated Mn thickness range.

The oxidized sample was obtained by exposing it *in situ* to 20 L of O_2 at RT ($1 \text{ L} = 10^{-6}$ Torr s). A few representative XAS spectra at the Mn- $L_{2,3}$ edges of the oxidized Mn/Co/Cu(001) as a function of t_{Mn} are shown in Fig. 1(b). Both L_3 and L_2 edges, as a consequence of the oxidation, exhibit multiplet structures and a spectral shape which, at variance with the clean case, evolves with Mn thickness.

The t_{Mn} dependence of the XAS spectrum stems from the large sampling depth of this technique which makes it sensitive to both the topmost oxidized layers and the buried portion of the Mn film unaffected by the oxidation process. The spectra are therefore a superposition of oxide and metallic spectra with the metallic contribution which becomes increasingly

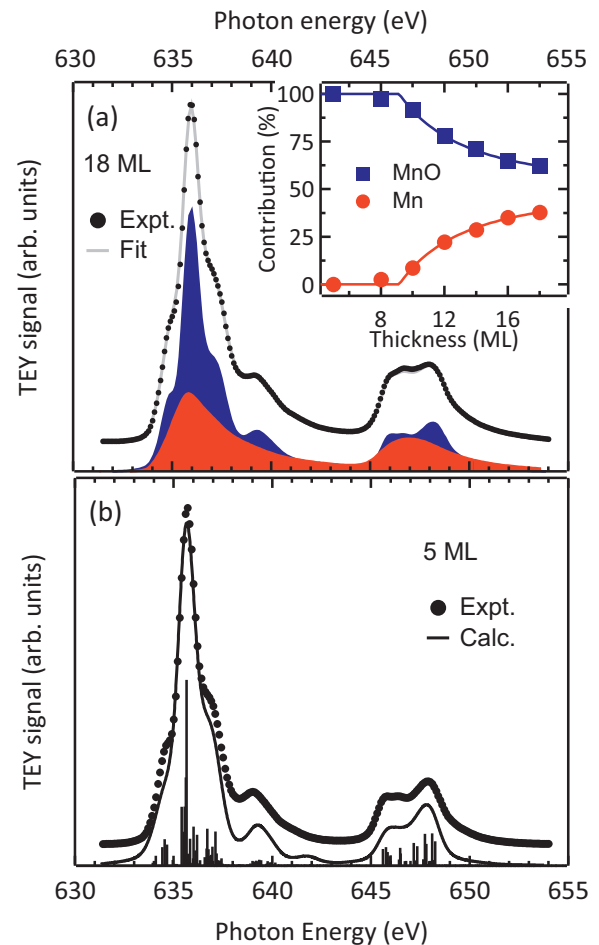


FIG. 2. (Color online) (a) Experimental (black circles) and fit (solid gray line) XAS spectra at the Mn- $L_{2,3}$ edges for the 18-ML-thick oxidized Mn overlayer on Co/Cu(001). The blue (orange) area depicts the oxide (metallic) spectral contribution. Inset: fractions of the metallic (orange circles) and oxide (blue squares) contribution to the total XAS spectra (see text for details). (b) Experimental (markers) and calculated (solid line) XAS spectra at the Mn- $L_{2,3}$ edges (see text for details).

more relevant moving from low to high Mn thickness. The thickness-dependent spectra can be therefore fitted as the weighted sum of the metallic and oxide spectra and the t_{Mn} dependence of the relative weights of the metal/oxide fraction can be exploited to assess the thickness of the Mn oxide. To this end, we assumed that the thinnest investigated Mn thickness (5 ML) is fully oxidized and that the oxide grows homogeneously to the detriment of the Mn film, as sketched in the inset of Fig. 1(b). The as-deposited 18-ML-thick and the oxidized 5-ML-thick spectra shown in Fig. 1, normalized to the integral of their intensities, were therefore chosen as references for the metallic and oxide spectra. As an example, in Fig. 2(a), we report the result of the fit of the XAS spectrum for the 18-ML-thick oxidized Mn/Co system where the metallic and oxide contributions are reported as the orange and blue areas, respectively. The t_{Mn} dependence of the relative weight of the metallic and oxide spectra are shown in the inset of Fig. 2(a). The oxide fraction, starting from 100%, begins to gradually decrease from $t_{\text{Mn}} \approx 8$ ML onwards, down to

60% for highest investigated thickness. Correspondingly, the metal fraction, starting from 0%, begins rising at $t_{\text{Mn}} \approx 8$ ML, reaching about 40% at high Mn thickness. The tendency to saturate for increasing thickness is clearly due to the finite, albeit large, probing depth of XAS.

The equivalent thickness of the Mn film that turned to oxide following the O_2 exposure has been deduced by fitting the metallic and oxide percentages vs initial Mn thickness with a model which assumes a uniform oxide thickness and takes into account the inelastic mean free path (IMFP) in the metallic layer. The result of the fit, shown in the inset of Fig. 2(a), gives a thickness of the oxide layer of about 9 ML and an IMFP in the metallic Mn of 1.2 ± 0.2 nm, close to the IMFP found in transition metals [20]. Since uniform oxidation has been assumed, the IMFP in the oxide layer does not influence the metallic and oxide percentages evolution with Mn thickness and cannot be extracted by the fitting procedure.

In order to identify the type of oxide which formed following the exposure to oxygen, in Fig. 2(b) we compare the experimental XAS spectrum for the oxidized 5-ML-thick Mn film with the theoretical spectrum calculated from the ideal multiplet structure of Mn(II) [21]. The calculated curve results from a convolution of the theoretical absorption multiplets for the +2 valence state (black sticks) with a Lorentzian function of width 0.2 eV for L_3 and 0.3 eV for L_2 , which takes into account the lifetime of each state, and an overall Gaussian function of 0.3 eV full width at half maximum (FWHM) accounting for the experimental resolution. [22] Calculation have been performed in octahedral (O_h) symmetry with the crystal-field parameter $10 Dq = 0.8$ eV and the $2p$ and $3d$ spin-orbit parameters equal to 6.98 and 0.03 eV, respectively. A reduction factor of the Slater integrals of 80% has been also included.

The sensitivity of XAS to the valence state of the absorbing ion through the peculiar multiplet structures [23] provides a clear-cut evidence for the identification of the oxide as MnO [21,24], which is an AF material with a Néel temperature $T_N = 118$ K, much lower than the measurement temperature (RT) for the magnetic characterization [25,26]. The whole oxidation to MnO of the 5-ML-thick Mn film upon exposure to oxygen and the lack of residual metallic Mn are further supported by the comparison of the XAS spectrum with those reported in Refs. [27,28].

In order to investigate the effects of oxidation on the EB properties of the films, hysteresis loops were measured by means of longitudinal MOKE. Exchange bias was established by subjecting the pristine film to FC from 420 K to RT, in an external magnetic field of 600 Oe aligned along the in-plane [110] direction of the Cu substrate. Hysteresis loops were measured at RT with the incidence plane parallel to the FC direction. After oxidation, the hysteresis loops were again measured *without* any further FC. Representative MOKE hysteresis loops recorded for the as-deposited and oxidized Mn/Co/Cu(001) wedge are reported in Figs. 3(a)–3(h). In Figs. 3(i)–3(j), we report the t_{Mn} dependence of the coercive (H_c) and exchange-bias fields (H_{EB}), before and after oxidation.

In the pristine case [Figs. 3(i)–3(j), full squares], H_c stays constant at about 40 Oe up to $t_{\text{Mn}} \approx 3$ ML, then steeply increases, reaching 200 Oe at $t_{\text{Mn}} \approx 9$ ML, and finally slowly

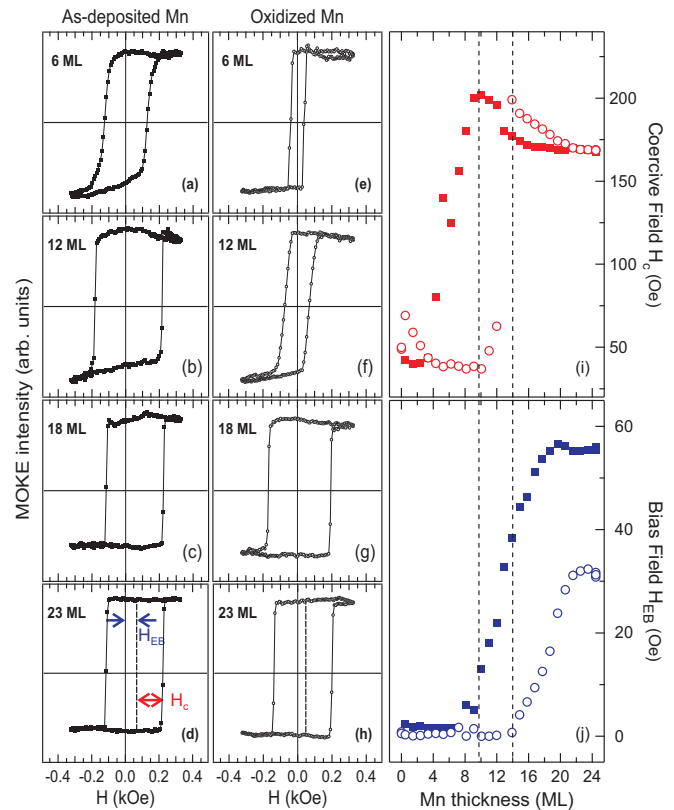


FIG. 3. (Color online) Hysteresis loops of exchange-biased Mn/Co/Cu(001) for a selected set of Mn thicknesses in the pristine state [(a)–(d)] and upon oxidation [(e)–(h)]. Comparison of H_c (i) and H_{EB} (j) of Mn/Co/Cu(001) vs Mn thickness before (full squares) and after oxidation (open circles). Dashed lines mark the correspondence between the onset of H_{EB} and the H_c maximum.

decreases towards a saturation value of about 170 Oe. H_{EB} stays zero up to $t_{\text{Mn}} \approx 8$ –9 ML, then starts rising exactly in correspondence of the H_c maximum. It then keeps increasing with increasing t_{Mn} , saturating at about 55 Oe for $t_{\text{Mn}} > 20$ ML.

According to the domain-state model of EB [2] and the t_{Mn} -dependent magnetic properties of Mn films grown on Co/Cu(001) [13,17,29], the t_{Mn} dependence of H_c can be interpreted as follows. In the case of a quasi-ideal epitaxial system like ours, the coercive field is chiefly determined by the depinning energy for domain-wall (DW) propagation. H_c thus starts to increase beyond 2 ML, when Mn films become fully AF [13,17,29]. For $2 < t_{\text{Mn}} < 8$ ML, where no EB appears, the increase of H_c can be related to the dragging of increasingly broad AF DWs by the corresponding DWs in the Co films, triggered by the magnetic-field sweeps. Around 8 ML, at the EB onset, an AF domain structure, stable against the sweeps of the Co magnetization and eventually responsible of the EB effect, begins forming in the Mn layer. From then onwards, an increase in the AF-layer thickness ceases to have a direct effect on H_c , and the pinning energy of the FM DWs, ultimately responsible for the coercive field, are ruled by the way AF domains reach out at the AF/FM interface, leading to a substantial t_{Mn} insensitivity of H_c . The gradual rise and saturation of H_{EB} with increasing t_{Mn} can be analogously interpreted in terms of

the gradual development of AF domains, with their associated PU-spin density, followed by the achievement of a steady-state configuration.

After oxidation, a pronounced change occurs in the t_{Mn} dependence of both H_c and H_{EB} [Figs. 3(i)–3(j), open circles]. At first sight, the oxidation induces a rigid upward thickness shift of the two curves, perfectly consistent with the formation of a surface paramagnetic Mn oxide layer to the detriment of metallic AF Mn. Looking at the curves in more detail, however, significant deviations from this simple picture can be observed. Concerning H_c , the maximum and saturation values of the oxidized system are comparable to the ones of the pristine Mn/Co/Cu(001). This observation is in agreement with the sole influence of the Mn/Co interface on the DW pinning energy, and thus the coercivity, which occurs from the onset of the EB onwards. However, whereas the maximum and saturation values of H_c are comparable for the as-deposited and oxidized Mn/Co/Cu(001), the H_c increase is steeper in the oxidized case, indicating a different t_{Mn} evolution of the AF internal magnetic structure (possibly domains) in the two samples. Concerning EB, we notice that the onset of H_{EB} still occurs in correspondence with the maximum of H_c , suggesting this to be a general feature [3], solely related to the formation of AF domains [2]. However, at variance with H_c , H_{EB} saturates at about 30 Oe, much lower than the pristine case, and this value did not further change upon subsequent FC procedures. This result cannot be accounted for by the mere formation of a surface paramagnetic layer, which would have resulted in the shift of the thickness behavior of H_c and H_{EB} , but requires that the formation of the MnO layer actively influences the EB properties of the system, significantly reducing the saturation value of the EB field which is reached at high Mn thickness. Taking into account the essential role played by the PU spin in the AF layer, the change of the outer interface of the AF layer from metal/vacuum to metal/oxide appears to influence the magnetic structure of the AF layer as a whole and, consequently, to affect the PU-spin density responsible for the EB effect. A possible physical mechanism for this to occur is the enhanced magnetic anisotropy (MA) of clean metallic surfaces. In the parent case of Mn/Cu₃Au, for example, a very strong Mn surface anisotropy was found, compared to a negligible bulk anisotropy [30]. Given the influence of the MA in determining the DW characteristics, a change of the surface MA due to oxidation could correspondingly modify the DW configuration in the AF, hence the PU-spin density and eventually the EB.

In conclusion, we have shown that surface modifications induced by controlled exposure to oxygen have a sizable effect on the EB properties of Mn/Co/Cu(001) bilayers. Our data suggest that in appropriate cases, the magnetic characteristics of the AF near-surface region might influence the density of pinned uncompensated spins responsible for the EB effect. In this respect, our finding has a potential impact on both fundamental and technological aspects of EB, suggesting that nonmagnetic capping layers might affect the EB, and opening the way to the engineering of either the capping layers or the free surfaces for tailoring the EB in scientific samples or devices.

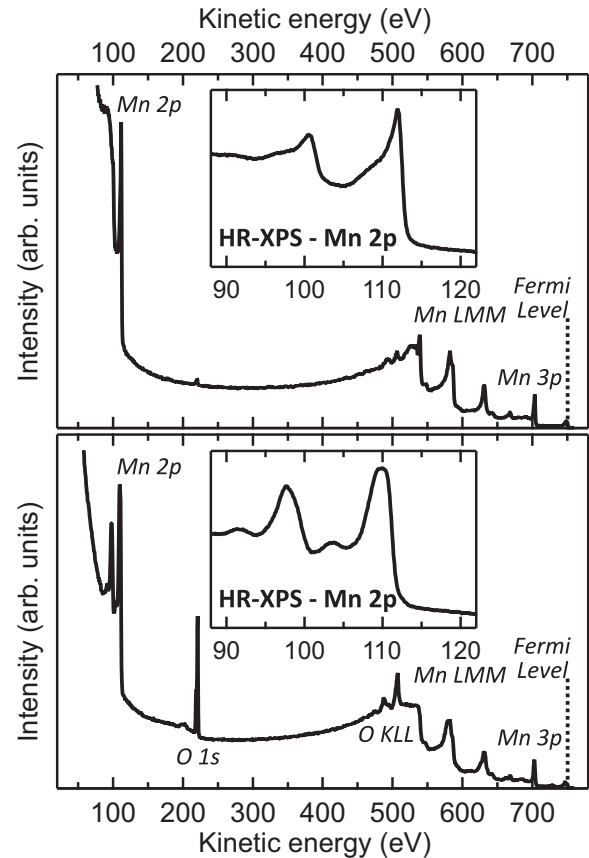


FIG. 4. XPS spectra of the as-deposited (top panel) and oxidized (bottom panel) Mn/Co/Cu(001). The spectra refer to a thickness of the Mn overlayer of about 18 ML. The insets show a HR-XPS spectra closeup of the Mn 2*p* doublet. XPS spectra were taken with a photon energy of 750 eV and an angle of incidence of 45°. Photoemitted electrons were collected at normal incidence.

Financial support from Consiglio Nazionale delle Ricerche (CNR), through the Italian-Taiwanese Bilateral Projects Program, from the University of Genova (Projects No. PRA 2011 and No. PRA 2012) and MIUR (Project No. PRIN 2008AKZSXY_002) is acknowledged. Frank M. F. de Groot is gratefully acknowledged for developing and distributing the CTM4XAS program.

APPENDIX: XPS ANALYSIS

In Fig. 4, XPS spectra of the as-deposited (top panel) and oxidized (bottom panel) Mn/Co/Cu(001) are shown.

In the as-deposited Mn/Co/Cu(001) sample, only traces of oxygen can be detected. The Mn2*p* peaks of the oxidized Mn/Co/Cu(001) sample and, in particular, the energy position of the satellite structure between the Mn2*p*_{3/2} and Mn2*p*_{1/2} agree with those reported for MnO in Ref. [31]. It is worth noting that, at variance with the XAS spectra shown in Fig. 1(b), the XPS spectra of the oxidized samples do not depend on the thickness of the Mn overlayer. This is due to the limited sampling depth of XPS which thus prevents its use for the assessment of the thickness of the Mn film that turned to oxide following the O₂ exposure.

- [1] W. H. Meiklejohn and C. P. Bean, *Phys. Rev.* **102**, 1413 (1956).
- [2] A. P. Malozemoff, *Phys. Rev. B* **35**, 3679 (1987).
- [3] J. Nogués and I. K. Schuller, *J. Magn. Magn. Mater.* **192**, 203 (1999).
- [4] A. E. Berkowitz and K. Takano, *J. Magn. Magn. Mater.* **200**, 552 (1999).
- [5] J. Nogués, J. Sort, V. Langlais, V. Skumryev, S. S. Suriñach, J. M. Muñoz, and M. Baró, *Phys. Rep.* **422**, 65 (2005).
- [6] H. Ohldag, A. Scholl, F. Nolting, E. Arenholz, S. Maat, A. T. Young, M. Carey, and J. Stöhr, *Phys. Rev. Lett.* **91**, 017203 (2003).
- [7] S. Roy, M. R. Fitzsimmons, S. Park, M. Dorn, O. Petravic, I. V. Roshchin, Z.-P. Li, X. Battle, R. Morales, A. Misra, X. Zhang, K. Chesnel, J. B. Kortright, S. K. Sinha, and I. K. Schuller, *Phys. Rev. Lett.* **95**, 047201 (2005).
- [8] M. R. Fitzsimmons, B. J. Kirby, S. Roy, Z.-P. Li, I. V. Roshchin, S. K. Sinha, and I. K. Schuller, *Phys. Rev. B* **75**, 214412 (2007).
- [9] S. Brück, G. Schütz, E. Goering, X. Ji, and K. M. Krishnan, *Phys. Rev. Lett.* **101**, 126402 (2008).
- [10] S. Doi, N. Awaji, K. Nomura, T. Hirono, T. Nakamura, and H. Kimura, *Appl. Phys. Lett.* **94**, 232504 (2009).
- [11] M. Bode, E. Y. Vedmedenko, K. V. Bergmann, A. Kubetza, P. Ferriani, S. Heinze, and R. Wiesendanger, *Nat. Mater.* **5**, 477 (2006).
- [12] R. Morales, Z.-P. Li, J. Olamit, K. Liu, J. M. Alameda, and I. K. Schuller, *Phys. Rev. Lett.* **102**, 097201 (2009).
- [13] J. T. Kohlhepp and W. J. M. de Jonge, *Phys. Rev. Lett.* **96**, 237201 (2006).
- [14] J. T. Kohlhepp, H. Wieldraaijer, and W. J. M. de Jonge, *Appl. Phys. Lett.* **89**, 032507 (2006).
- [15] P.-J. Hsu, C.-I. Lu, Y.-H. Chu, B.-Y. Wang, C.-B. Wu, L.-J. Chen, S.-S. Wong, and M.-T. Lin, *Phys. Rev. B* **85**, 174434 (2012).
- [16] C.-B. Wu, J. Song, and W. Kuch, *Appl. Phys. Lett.* **101**, 012404 (2012).
- [17] M. Caminale, R. Moroni, P. Torelli, W. C. Lin, M. Canepa, L. Mattera, and F. Bisio, *Phys. Rev. Lett.* **112**, 037201 (2014).
- [18] F. Bisio, S. Terreni, M. Canepa, and L. Mattera, *Phys. Rev. B* **72**, 174413 (2005).
- [19] G. Panaccione *et al.*, *Rev. Sci. Instrum.* **80**, 043105 (2009).
- [20] C. J. Powell and A. Jablonski, *J. Phys. Chem. Ref. Data* **28**, 19 (1999).
- [21] R. Moroni, P. Ghigna, D. Bonacchi, A. Caneschi, and D. Rovai, *Inorg. Chim. Acta* **361**, 3887 (2008).
- [22] E. Stavitski and F. M. de Groot, *Micron* **41**, 687 (2010).
- [23] R. Moroni, C. Cartier dit Moulin, G. Champion, M.-A. Arrio, P. Sainctavit, M. Verdagner, and D. Gatteschi, *Phys. Rev. B* **68**, 064407 (2003).
- [24] H. Ikeno, T. Mizoguchi, and I. Tanaka, *Phys. Rev. B* **83**, 155107 (2011).
- [25] C. G. Shull, W. A. Strauser, and E. O. Wollan, *Phys. Rev.* **83**, 333 (1951).
- [26] J. E. Pask, D. J. Singh, I. I. Mazin, C. S. Hellberg, and J. Kortus, *Phys. Rev. B* **64**, 024403 (2001).
- [27] B. Gilbert, B. H. Frazer, A. Belz, P. G. Conrad, K. H. Neelson, D. Haskel, J. C. Lang, G. Srajer, and G. De Stasio, *J. Phys. Chem. A* **107**, 2839 (2003).
- [28] V. Bayer, R. Podloucky, C. Franchini, F. Allegretti, B. Xu, G. Parteder, M. G. Ramsey, S. Surnev, and F. P. Netzer, *Phys. Rev. B* **76**, 165428 (2007).
- [29] W. L. O'Brien and B. P. Tonner, *Phys. Rev. B* **50**, 2963 (1994).
- [30] C. L. Gao, A. Ernst, G. Fischer, W. Hergert, P. Bruno, W. Wulfhekel, and J. Kirschner, *Phys. Rev. Lett.* **101**, 167201 (2008).
- [31] V. D. Castro and G. Polzonetti, *J. Electron Spectrosc. Relat. Phenom.* **48**, 117 (1989).